NLO effects in EFT fits to W^+W^- production at the LHC

Julien Baglio,[1,*] Sally Dawson,[2,†] and Ian M. Lewis[3,‡]
[1]Institute for Theoretical Physics, University of Tübingen, Auf der Morgenstelle 14, 72076 Tübingen, Germany
[2]Department of Physics, Brookhaven National Laboratory, Upton, New York 11973, USA
[3]Department of Physics and Astronomy, University of Kansas, Lawrence, Kansas 66045, USA

(Received 10 December 2018; published 20 February 2019)

We study the impact of anomalous gauge boson and fermion couplings on the production of W^+W^- pairs at potential future LHC upgrades and estimate the sensitivity at $\sqrt{S} = 14$ TeV with 3 ab^{-1} and $\sqrt{S} = 27$ TeV with 15 ab^{-1}. A general technique for including next-to-leading order (NLO) QCD effects in effective field theory (EFT) fits to kinematic distributions is presented, and numerical results are given for $\sqrt{S} = 13$ TeV W^+W^- production. Our method allows fits to anomalous couplings at NLO accuracy in any EFT basis and has been implemented in a publicly available version of the POWHEG-BOX. Analytic expressions for the K-factors relevant for 13 TeV total cross sections are given for the Hagiwara-Ishihara-Szalapski-Zeppenfeld and Warsaw EFT bases and differential K-factors can be obtained using the Supplemental Material. Our study demonstrates the necessity of including anomalous Z-fermion couplings in the extraction of limits on anomalous three-gauge-boson couplings.

DOI: 10.1103/PhysRevD.99.035029

I. INTRODUCTION

With the discovery of the Higgs boson, and subsequent measurements of its properties at the LHC, the general features of the Standard Model (SM) electroweak theory have been confirmed experimentally [1]. Measurements of the Higgs couplings and production rates agree with SM predictions at the 10%–20% level [2–6] and there is no indication of the existence of any new particle at the TeV scale. Going forward, the task is to make comparisons between theory and data at the few-percent level. This requires not only high-luminosity LHC running, but also improved theoretical calculations. Furthermore, Higgs physics cannot be studied in isolation, but must be examined in the context of the entire set of SM interactions.

W^+W^- pair production is an example of a process whose properties are highly restricted by LEP measurements [7], yet still provides relevant information about the Higgs sector from LHC data. The production of W^+W^- pairs provides a sensitive test of the electroweak gauge structure, since in the SM there are delicate cancellations between contributions from s-channel γ and Z exchange and t-channel fermion exchange that maintain perturbative unitarity. Deviations from the form of the γW^+W^- and ZW^+W^- vertices predicted by the SM spoil the cancellations between contributions that enforce unitarity. These deviations have been studied for decades [8,9], while the importance of non-SM fermion-Z interactions in ensuring unitarity in W^+W^- pair production has only recently been realized [10–13].

Beyond the Standard Model (BSM) physics effects in W^+W^- production can be studied using effective Lagrangian techniques where the new physics is parametrized as an operator expansion in inverse powers of a high scale, Λ,

$$L_{\mathrm{SMEFT}} = L_{\mathrm{SM}} + \sum_{i,n} \frac{C_i^{(n)}}{\Lambda^{n-4}} O_i^{(n)} + \ldots \qquad (1)$$

where $O_i^{(n)}$ has mass dimension-n and L_{SM} contains the complete SM Lagrangian. The subscript SMEFT denotes the SM effective field theory where the Higgs is assumed to be part of an $SU(2)$ doublet. This approach further assumes that there are no new light degrees of freedom. Neglecting flavor, there are 59 possible operators at dimension-6 [14,15], but only a small subset of these contribute to W^+W^- production. At high energies, the longitudinally polarized contributions to W^+W^- grow with energy faster than the SM contributions in the presence of BSM physics. This implies that the LHC can put strong constraints on the coefficients of the dimension-6 SMEFT operators.

*julien.baglio@uni-tuebingen.de
†dawson@bnl.gov
‡ian.lewis@ku.edu

We consistently work with a dimension-6 Lagrangian. At dimension-8, there are many other possible operators, not only modifying the triple-gauge-boson interactions but also new four-point ggW^+W^- interactions [16]. These operators contribute at tree level at order $\mathcal{O}(1/\Lambda^4)$ in the EFT and must be included in a study of the dimension-8 Lagrangian. However, the study of dimension-8 operators is beyond the scope of this work, so that we do not consider operators modifying the partonic cross section $gg \to W^+W^-$.

The effects of new physics contributions to W^+W^- gauge boson pair production can be expected to be of the same order of magnitude as QCD corrections, and so these contributions must be included when extracting limits on new physics. QCD effects in the effective field theory can also change the dependence of the experimental kinematic distributions on the coefficients of Eq. (1). The SM QCD corrections to W^+W^- pair production are known up to next-to-next-to leading order (NNLO) [17,18], including the effects of a jet veto [19,20], and the electroweak corrections exist at next-to-leading order (NLO) [21–23]. The SM and dimension-6 gg initial state contributions are formally NNLO and are not included, although at 14 TeV they increase the cross section by roughly 10% (see e.g., Refs. [24,25]). We perform an analysis including QCD corrections [26,27] at NLO in the SMEFT, along with modifications of both the three-gauge-boson and fermion couplings, extending our previous study [11] by including the leptonic decays of the W's. The effects of anomalous three-gauge-boson couplings exist in the POWHEG-BOX framework [28,29], and we add the additional contributions from anomalous fermion couplings. This public tool can be found at [30] and can be used to perform fits to anomalous couplings including NLO QCD and showering effects.

In Sec. II, we review the basics of the effective field theory framework for W pair production and discuss the effects of NLO QCD in the SMEFT. The determination of NLO QCD effects in a theory with anomalous couplings has typically been done on a case by case basis, or alternatively by allowing one SMEFT coupling at a time to vary. In Sec. II B, we present a general method for deriving NLO expressions for the total cross section and for distributions in a SMEFT in terms of a fixed number of subamplitudes, which we term "primitive cross sections." These results can be used to obtain either total or differential K-factors in any SMEFT basis. In Sec. III, we compare projections for the measurements of anomalous three-gauge-boson couplings at the high-luminosity LHC with those of a future 27 TeV collider and demonstrate the critical importance of including anomalous fermion couplings in the fits (see also Ref. [31] for SMEFT projections in a global fit at a 27 TeV hadron collider). We provide numerical results in Sec. IV for K-factors for the leading lepton p_T ($p_T^{\ell,\mathrm{lead}}$) and m_{ll} distributions for $W^+W^- \to e^\pm\mu^\mp\nu\bar{\nu}$ at 13 TeV as an illustration of our technique, along with analytic results for the total cross section, as functions of arbitrary EFT coefficients.

II. BASICS

A. Effective gauge and fermion interactions

Assuming CP conservation, the most general Lorentz invariant three-gauge-boson couplings are [9,32]

$$\mathcal{L}_V = -ig_{WWV}\Big[g_1^V(W^+_{\mu\nu}W^{-\mu}V^\nu - W^-_{\mu\nu}W^{+\mu}V^\nu) + \kappa^V W^+_\mu W^-_\nu V^{\mu\nu} + \frac{\lambda^V}{M_W^2}W^+_{\rho\mu}W^{-\mu}{}_\nu V^{\nu\rho}\Big], \tag{2}$$

where $V = \gamma, Z$; $g_{WW\gamma} = e$; and $g_{WWZ} = g\cos\theta_W$, with θ_W being the weak mixing angle ($s_W \equiv \sin\theta_W$, $c_W \equiv \cos\theta_W$). The fields in Eq. (2) are the canonically normalized mass eigenstate fields. We define $g_1^V = 1 + \delta g_1^V$, $\kappa^V = 1 + \delta\kappa^V$ and in the SM $\delta g_1^V = \delta\kappa^V = \lambda^V = 0$. Gauge invariance requires $\delta g_1^\gamma = 0$.

The effective couplings of quarks to gauge fields can be written as[1] (assuming no new tensor structures)

$$\mathcal{L} \equiv g_Z Z_\mu[g_L^{Zq} + \delta g_L^{Zq}]\bar{q}_L\gamma_\mu q_L + g_Z Z_\mu[g_R^{Zq} + \delta g_R^{Zq}]\bar{q}_R\gamma_\mu q_R + \frac{g}{\sqrt{2}}\{W_\mu[(1+\delta g_L^W)\bar{u}_L\gamma_\mu d_L + \delta g_R^W\bar{u}_R\gamma_\mu d_R] + \mathrm{H.c.}\}, \tag{3}$$

where $g_Z = e/(c_W s_W) = g/c_W$, Q_q is the electric charge of the quarks, and q denotes up-type or down-type quarks. We assume that the anomalous fermion couplings, $\delta g_{L,R}^{Zq}$, along with the anomalous W-fermion couplings, are flavor independent. We also neglect Cabbibo-Kobayashi-Maskawa (CKM) mixing. The SM quark couplings are

$$g_R^{Zq} = -s_W^2 Q_q \quad \text{and} \quad g_L^{Zq} = T_3^q - s_W^2 Q_q, \tag{4}$$

with $T_3^q = \pm\frac{1}{2}$. $SU(2)$ invariance implies

$$\delta g_L^W = \delta g_L^{Zu} - \delta g_L^{Zd}, \quad \delta g_1^Z = \delta\kappa^Z + \frac{s_W^2}{c_W^2}\delta\kappa^\gamma, \quad \lambda^\gamma = \lambda^Z. \tag{5}$$

This framework leads to seven unknown parameters: $\delta g_1^Z, \delta\kappa_Z, \lambda_Z, \delta g_L^{Zu}, \delta g_L^{Zd}, \delta g_R^{Zu}$ and δg_R^{Zd}.[2]

[1] We assume SM gauge couplings to leptons, since these couplings are highly restricted by LEP data.

[2] We neglect possible anomalous right-handed W-quark couplings, since they are suppressed by small Yukawa couplings in an maximal flavor violating (MFV) framework.

At high energy scales the dominant contributions to W^+W^- come from longitudinally polarized W's. Keeping only the terms linear in the anomalous couplings, the amplitudes $\mathcal{A}_{rr'\lambda\lambda'}$ for $\bar{q}_r q_{r'} \to W^+_\lambda W^-_{\lambda'}$, where r, r', λ, λ' label the respective particle helicities, have the high energy limits [9,11–13,32–34]

$$\begin{aligned}\mathcal{A}_{+-00} &\to \frac{g^2 s}{2M_W^2}\sin\theta\{\delta\kappa^Z(s_W^2 Q_q - T_3^q) \\ &\quad - s_W^2 Q_q \delta\kappa^\gamma - \delta g_L^{Zq} + 2T_3^q \delta g_L^W\}, \\ \mathcal{A}_{-+00} &\to \frac{g^2 s}{2M_W^2}\sin\theta\{s_W^2 Q_q(\delta\kappa^\gamma - \delta\kappa^Z) + \delta g_R^{Zq}\}, \quad (6)\end{aligned}$$

where $\sqrt{s}$ is the partonic subenergy. From Eq. (6), it is clear that the longitudinal polarizations do not depend on the full range of seven anomalous couplings, but on four linear combinations when u and d contributions are included. Note that the dependence on λ_Z is subleading in s. The transverse polarizations have a weaker dependence on the energy scale and different dependencies on the anomalous couplings.

The Lagrangians of Eqs. (2) and (3) can be mapped onto the effective Lagrangian of Eq. (1). For future convenience, we consider the mapping to the Warsaw basis [15,35] and the Hagiwara-Ishihara-Szalapski-Zeppenfeld (HISZ) basis [9]. In the Warsaw basis [15], the dimension-6 operators relevant for our analysis are

$$\begin{aligned}&L_{\text{WARSAW}} \\ &= \frac{C_{3W}}{\Lambda^2}\epsilon^{abc} W_\mu^{a\nu} W_\nu^{b\rho} W_\rho^{c\mu} + \frac{C_{HD}}{\Lambda^2}|\Phi^\dagger(D_\mu\Phi)|^2 \\ &\quad + \frac{C_{HWB}}{\Lambda^2}\Phi^\dagger\sigma^a\Phi W_{\mu\nu}^a B^{\mu\nu} + \frac{C_{Hf}^{(3)}}{\Lambda^2} i(\Phi^\dagger \overleftrightarrow{D}_\mu^a \Phi)\bar{f}_L\gamma^\mu\sigma^a f_L \\ &\quad + \frac{C_{Hf}^{(1)}}{\Lambda^2} i(\Phi^\dagger \overleftrightarrow{D}_\mu \Phi)\bar{f}_L\gamma^\mu f_L + \frac{C_{Hf}}{\Lambda^2} i(\Phi^\dagger \overleftrightarrow{D}_\mu \Phi)\bar{q}_R\gamma^\mu q_R \\ &\quad + \frac{C_{Hud}}{\Lambda^2} i(\tilde{\Phi}^\dagger D_\mu\Phi)\bar{u}_R\gamma^\mu d_R + \frac{C_{ll}}{\Lambda^2}(\bar{l}_L\gamma^\mu l_L)(\bar{l}_L\gamma_\mu l_L), \quad (7)\end{aligned}$$

where f can be either a quark or a lepton, $D_\mu\Phi = (\partial_\mu - i\frac{g}{2}\sigma^a W_\mu^a - i\frac{g'}{2}B_\mu)\Phi$, $W_{\mu\nu}^a = \partial_\mu W_\nu^a - \partial_\nu W_\mu^a + g\varepsilon^{abc}W_\mu^b W_\nu^c$, $\Phi^\dagger \overleftrightarrow{D}_\mu \Phi = \Phi^\dagger D_\mu\Phi - (D_\mu\Phi^\dagger)\Phi$, and $\Phi^\dagger \overleftrightarrow{D}_\mu^a \Phi = \Phi^\dagger D_\mu\sigma^a\Phi - (D_\mu\Phi^\dagger)\sigma^a\Phi$. Φ stands for the Higgs doublet field with a vacuum expectation value $\langle\Phi\rangle = (0, v/\sqrt{2})^{\mathrm{T}}$.

In the HISZ basis, the fermion couplings are unchanged, while the three-gauge-boson couplings are

$$\begin{aligned}L_{\text{HISZ}} &= \frac{f_W}{\Lambda^2}(D_\mu\Phi)^\dagger \hat{W}^{\mu\nu} D_\nu\Phi + \frac{f_B}{\Lambda^2}(D_\mu\Phi)^\dagger \hat{B}^{\mu\nu} D_\nu\Phi \\ &\quad + \frac{f_{WWW}}{\Lambda^2}\mathrm{Tr}(\hat{W}_{\mu\nu}\hat{W}^{\nu\rho}\hat{W}_\rho^\mu), \quad (8)\end{aligned}$$

where $\hat{W}^{\mu\nu} = i\frac{g}{2}\sigma^a W^{a,\mu\nu}$ and $\hat{B}^{\mu\nu} = i\frac{g'}{2}B^{\mu\nu}$. Expressions for the anomalous three-gauge-boson couplings are given in Table I and for the anomalous fermion couplings in Table II.[3]

TABLE I. Anomalous three-gauge-boson couplings in the Warsaw [15] and HISZ [9]. δv is given in Table II.

	Warsaw basis	HISZ
δg_1^Z	$\frac{v^2}{\Lambda^2}\frac{1}{c_W^2 - s_W^2}(\frac{s_W}{c_W}C_{HWB} + \frac{1}{4}C_{HD} + \delta v)$	$\frac{M_Z^2}{2\Lambda^2}f_W$
$\delta\kappa^Z$	$\frac{v^2}{\Lambda^2}\frac{1}{c_W^2 - s_W^2}(2s_W c_W C_{HWB} + \frac{1}{4}C_{HD} + \delta v)$	$\frac{M_Z^2}{2\Lambda^2}(c_W^2 f_W - s_W^2 f_B)$
$\delta\kappa^\gamma$	$-\frac{v^2}{\Lambda^2}\frac{c_W}{s_W}C_{HWB}$	$\frac{M_W^2}{2\Lambda^2}(f_W + f_B)$
λ^γ	$\frac{v}{\Lambda^2}3M_W C_{3W}$	$\frac{3g^2M_W^2}{4\Lambda^2}f_{WWW}$
λ^Z	$\frac{v}{\Lambda^2}3M_W C_{3W}$	$\frac{3g^2M_W^2}{4\Lambda^2}f_{WWW}$

TABLE II. Anomalous fermion couplings in the Warsaw [15] basis.

	Warsaw basis
δg_L^{Zu}	$-\frac{v^2}{2\Lambda^2}(C_{Hq}^{(1)} - C_{Hq}^{(3)}) + \frac{1}{2}\delta g_Z + \frac{2}{3}(\delta s_W^2 - s_W^2\delta g_Z)$
δg_L^{Zd}	$-\frac{v^2}{2\Lambda^2}(C_{Hq}^{(1)} + C_{Hq}^{(3)}) - \frac{1}{2}\delta g_Z - \frac{1}{3}(\delta s_W^2 - s_W^2\delta g_Z)$
δg_R^{Zu}	$-\frac{v^2}{2\Lambda^2}C_{Hu} + \frac{2}{3}(\delta s_W^2 - s_W^2\delta g_Z)$
δg_R^{Zd}	$-\frac{v^2}{2\Lambda^2}C_{Hd} - \frac{1}{3}(\delta s_W^2 - s_W^2\delta g_Z)$
δg_L^W	$\frac{v^2}{\Lambda^2}C_{Hq}^{(3)} + c_W^2\delta g_Z + \delta s_W^2$
δg_Z	$-\frac{v^2}{\Lambda^2}(\delta v + \frac{1}{4}C_{HD})$
δv	$C_{Hl}^{(3)} - \frac{1}{2}C_{ll}$
δs_W^2	$-\frac{v^2}{\Lambda^2}\frac{s_W c_W}{c_W^2 - s_W^2}[2s_W c_W(\delta v + \frac{1}{4}C_{HD}) + C_{HWB}]$

B. Primitive cross sections

We want to compute differential and total cross sections for a hadronic scattering process at NLO QCD for arbitrary anomalous couplings. Since these calculations can be numerically intensive, it is desirable not to have to repeat the calculation over and over again for different values of the anomalous couplings. Here we discuss a technique for generating results in terms of a set of primitive cross sections which need to be calculated only once for a given process and set of cuts. The primitive cross sections can be reweighted to allow for rapid scans over the anomalous couplings at NLO order.

Consider an arbitrary differential cross section $d\sigma^n(\vec{C})$ that is calculated to $\mathcal{O}(\Lambda^{-2n})$. It depends on m EFT coefficients $\vec{C} = (C_1, C_2, \ldots, C_m)$ and the relevant momenta, $\vec{p}$. We assume $C_i \sim \mathcal{O}(\Lambda^{-2})$. It is important to note that in general $d\sigma^4$ is the cross section to order $\mathcal{O}(\Lambda^{-4})$, but is not the amplitude squared. When both Z-fermion and three-gauge-boson (3 GB) couplings are nonzero, the amplitude squared contains terms up to $\mathcal{O}(\Lambda^{-8})$.

[3]We neglect dipole operators since they do not interfere with the SM contributions.

Calculating the cross section to $\mathcal{O}(\Lambda^{-2})$,

$$d\sigma^1(\vec{C}) \equiv d\sigma_{\rm SM}(1-\Sigma_{i=1}^m C_i) + \Sigma_{i=1}^m C_i d\sigma(1;\vec{R}_i), \quad (9)$$

where $\vec{R}_i$ are m-dimensional vectors with $\vec{R}_1 = (1,0,0\ldots..0)$; $\vec{R}_2 = (0,1,0\ldots.)$; $\vec{R}_m = (0,0\ldots.1)$; etc. The primitive cross section $d\sigma(n;\vec{R}_i)$ is the cross section obtained to arbitrary order $\mathcal{O}(\Lambda^{-2n})$ when $C_i = 1$ and all other $C_j = 0$, $j \neq i$:

$$d\sigma(n;\vec{R}_i) \equiv d\sigma^n(\vec{C} = \vec{R}_i). \quad (10)$$

The SM cross section with $\vec{C} = 0$ is $d\sigma_{\rm SM}$. For the process $pp \to W^+W^-$ under consideration here, there are seven primitive cross sections, $d\sigma(1;\vec{R}_i)$, when considering both anomalous 3 GB couplings and anomalous Z-fermion couplings, while there are only three when the fermion couplings take their SM values. Equation (9) holds bin by bin for differential rates and also for the total rate.

The procedure becomes significantly more laborious if the cross section is computed to $\mathcal{O}(\Lambda^{-4})$. We define m-dimensional vectors $\vec{M}_{ij}$, with $\vec{M}_{12} = (1,1,0,\ldots 0)$; $\vec{M}_{13} = (1,0,1\ldots.0)$; $\vec{M}_{23} = (0,1,1,\ldots.)$; etc. To $\mathcal{O}(\Lambda^{-4})$, the cross section decomposes into the primitive cross sections as

$$\begin{aligned} d\sigma^2(\vec{C}) = {} & d\sigma_{\rm SM}(1-\Sigma_{i=1}^m C_i) + \Sigma_i C_i d\sigma(1;\vec{R}_i) \\ & + \Sigma_{i=1}^m C_i^2 (d\sigma(2;\vec{R}_i) - d\sigma(1;\vec{R}_i)) \\ & + \Sigma_{i>j=1}^m C_i C_j [d\sigma(2;\vec{M}_{ij}) - d\sigma(2;\vec{R}_i) \\ & - d\sigma(2;\vec{R}_j) + d\sigma_{\rm SM}]. \end{aligned} \quad (11)$$

Evaluating the cross section with two nonzero C_i coefficients, $C_i = 1$, $C_j = 1$, and $C_{k\ell} = 0$ if $j \neq i$ or $k \neq \ell$, to arbitrary order $\mathcal{O}(\Lambda^{-2n})$ yields the primitive cross sections

$$d\sigma(n;\vec{M}_{ij}) \equiv d\sigma^n(\vec{C} = \vec{M}_{ij}). \quad (12)$$

We can calculate the primitive cross sections $d\sigma(n;\vec{R}_i)$ and $d\sigma(n;\vec{M}_{ij})$ once and then apply Eq. (11) to get the general result for arbitrary anomalous couplings. Equations (9) and (11) hold separately for LO and NLO corrected rates. For $pp \to W^+W^-$, there are 35 primitive cross sections at $\mathcal{O}(\Lambda^{-4})$ with both anomalous 3 GB couplings and anomalous fermion couplings nonzero.

Suppose we calculate the primitive cross sections in terms of a set of EFT parameters, $\vec{C} = (C_1,\ldots,C_m)$, but we want the results in terms of a different EFT basis, $\vec{C}' = (C_1',\ldots,C_m')$. The procedure is straightforward. We begin by considering two anomalous couplings, $m = 2$, and the $\mathcal{O}(\Lambda^{-2})$ case. The physical rate must be independent of the basis choice and, using the master formula of Eq. (9) for the two different bases,

$$\begin{aligned} d\sigma^1(\vec{C}) &= d\sigma_{\rm SM}(1-C_1-C_2) + C_1 d\sigma(1;\vec{R}_1) \\ &\quad + C_2 d\sigma(1;\vec{R}_2) \\ d\sigma^1(\vec{C}') &= d\sigma_{\rm SM}(1-C_1'-C_2') + C_1' d\sigma'(1;\vec{R}_1) \\ &\quad + C_2' d\sigma'(1;\vec{R}_2). \end{aligned} \quad (13)$$

The unprimed primitive cross sections are defined according to Eq. (10). To order $\mathcal{O}(\Lambda^{-2n})$ the primed primitive cross sections $d\sigma'(n,\vec{R}_i\prime)$ are defined with the vector $\vec{R}_i$ evaluated relative to the new basis $\vec{C}'$:

$$d\sigma'(n;\vec{R}_i) \equiv d\sigma^n(\vec{C}' = \vec{R}_i). \quad (14)$$

We need the $d\sigma'$'s in terms of the already computed $d\sigma$'s so that we can avoid recalculating the cross sections. Including a complete basis of dimension-6 operators, the input parameters are related by a linear transformation,

$$\begin{pmatrix} C_1 \\ C_2 \end{pmatrix} = \alpha \begin{pmatrix} C_1' \\ C_2' \end{pmatrix}, \quad (15)$$

where α is a 2×2 matrix. The $d\sigma'$ matrices are

$$\begin{aligned} d\sigma'(1;\vec{R}_1) &= d\sigma_{\rm SM}(1-\alpha_{11}-\alpha_{21}) + \alpha_{11} d\sigma(1;\vec{R}_1) \\ &\quad + \alpha_{21} d\sigma(1;\vec{R}_2) \end{aligned} \quad (16)$$

$$\begin{aligned} d\sigma'(1;\vec{R}_2) &= d\sigma_{\rm SM}(1-\alpha_{12}-\alpha_{22}) + \alpha_{12} d\sigma(1;\vec{R}_1) \\ &\quad + \alpha_{22} d\sigma(2;\vec{R}_2). \end{aligned} \quad (17)$$

Now consider the general case of a change of EFT input basis. Assume we have two minimum sets[4] of independent parameters $\vec{C} = (C_1, C_2, \ldots, C_m)$ and $\vec{C}' = (C_1', C_2', \ldots, C_m')$ that can be related linearly,

$$C_i = \sum_{j=1}^m \alpha_{ij} C_j', \qquad C_i' = \sum_{j=1}^m \alpha_{ij}^{-1} C_j, \quad (18)$$

where α^{-1} is the inverse matrix of α and α_{ij}^{-1} is its $\{i,j\}$th element.

Although the two parameter bases C_i, C_i' must give identical results for physical quantities and[5]

$$\sigma^n \equiv \sigma^n(\vec{C}) = \sigma^n(\vec{C}'), \quad (19)$$

the primitive cross sections are not the same since setting $C_i = 1$ is not the same as taking $C_i' = 1$. To $\mathcal{O}(\Lambda^{-2n})$, we define the primitive cross sections with two nonzero C_j' in the $\vec{C}'$ basis to be

[4]All redundant operators have been eliminated using the equations of motion.

[5]We suppress possible momentum dependence.

$$d\sigma'(2;\vec{M}_{ij}) \equiv d\sigma^n(\vec{C}' = \vec{M}'_{ij}) \tag{20}$$

where $\vec{M}_{ij}$ is evaluated relative to the $\vec{C}$ basis. The primitive cross sections $d\sigma(n;\vec{R}_i)$, $d\sigma(n;\vec{M}_{ij})$, and $d\sigma'(n;\vec{R}_j)$ are defined in Eqs. (10), (12), and (14), respectively.

The cross sections can now be expanded in terms of either set of parameters and primitive cross sections. At $\mathcal{O}(\Lambda^{-2})$, we have the cross sections[6]

$$\begin{aligned} d\sigma^1 &= d\sigma_{\mathrm{SM}} + \sum_{i=1}^{m} C_i(d\sigma(1;\vec{R}_i) - d\sigma_{\mathrm{SM}}) \\ &= d\sigma_{\mathrm{SM}} + \sum_{i=1}^{m} C'_i(d\sigma'(1;\vec{R}_i) - d\sigma_{\mathrm{SM}}), \end{aligned} \tag{21}$$

where σ_{SM} is the SM cross section with $\vec{C} = \vec{C}' = \vec{0}$. At order $\mathcal{O}(\Lambda^{-4})$, we have

$$\begin{aligned} d\sigma^2 &= d\sigma_{\mathrm{SM}} + \sum_{i=1}^{m} C_i(d\sigma(1;\vec{R}_i) - d\sigma_{\mathrm{SM}}) + \sum_{i=1}^{m} C_i^2(d\sigma(2;\vec{R}_i) - d\sigma(1;\vec{R}_i)) \\ &\quad + \Sigma_{i>j=1}^{m} C_i C_j(d\sigma(2;\vec{M}_{ij}) - d\sigma(2;\vec{R}_i) - d\sigma(2;\vec{R}_j) + d\sigma_{\mathrm{SM}}) \\ &= d\sigma_{\mathrm{SM}} + \sum_{i=1}^{m} C'_i(d\sigma'(1;\vec{R}_i) - d\sigma_{\mathrm{SM}}) + \sum_{i=1}^{m} C'^2_i(d\sigma'(2;\vec{R}_i) - d\sigma'(1;\vec{R}_i)) \\ &\quad + \Sigma_{i>j=1}^{m} C'_i C'_j(d\sigma'(2;\vec{M}_{ij}) - d\sigma'(2;\vec{R}_i) - d\sigma'(2;\vec{R}_j) + d\sigma_{\mathrm{SM}}). \end{aligned} \tag{22}$$

Finally, we find the relationships between the primitive cross sections using Eqs. (18), (21), and (22) that can be used to calculate cross sections in terms of an arbitrary EFT basis:

$$\begin{aligned} d\sigma'(1;\vec{R}_i) &= d\sigma_{\mathrm{SM}} + \sum_{k=1}^{m} \alpha_{ki}(d\sigma(1;\vec{R}_k) - d\sigma_{\mathrm{SM}}) \\ d\sigma'(2;\vec{R}_i) &= d\sigma'(1;\vec{R}_i) + \sum_{k=1}^{m} \alpha_{ki}^2(d\sigma(2;\vec{R}_k) - d\sigma(1;\vec{R}_k)) + \sum_{k>l=1}^{m} \alpha_{ki}\alpha_{li}(d\sigma(2;\vec{M}_{kl}) - d\sigma(2;\vec{R}_k) - d\sigma(2;\vec{R}_l) + d\sigma_{\mathrm{SM}}) \\ d\sigma'(2;\vec{M}_{ij}) &= d\sigma'(1;\vec{R}_i) + d\sigma'(1;\vec{R}_j) - d\sigma_{\mathrm{SM}} + \sum_{k=1}^{m} (\alpha_{ki} + \alpha_{kj})^2(d\sigma(2;\vec{R}_k) - d\sigma(1;\vec{R}_k)) \\ &\quad + \sum_{k>l=1}^{m} (\alpha_{ki} + \alpha_{kj})(\alpha_{li} + \alpha_{lj})(d\sigma(2;\vec{M}_{kl}) - d\sigma(2;\vec{R}_k) - d\sigma(2;\vec{R}_l) + d\sigma_{\mathrm{SM}}), \end{aligned} \tag{23}$$

or equivalently,

$$\begin{aligned} d\sigma(1;\vec{R}_i) &= d\sigma_{\mathrm{SM}} + \sum_{k=1}^{m} \alpha_{ki}^{-1}(d\sigma'(1;\vec{R}_k) - d\sigma_{\mathrm{SM}}) \\ d\sigma(2;\vec{R}_i) &= d\sigma(1;\vec{R}_i) + \sum_{k=1}^{m} (\alpha_{ki}^{-1})^2(d\sigma'(2;\vec{R}_k) - d\sigma'(1;\vec{R}_k)) + \sum_{k>l=1}^{m} \alpha_{ki}^{-1}\alpha_{li}^{-1}(d\sigma'(2;\vec{M}_{kl}) - d\sigma'(2;\vec{R}_k) - d\sigma'(2;\vec{R}_l) + d\sigma_{\mathrm{SM}}) \\ d\sigma(2;\vec{M}_{ij}) &= d\sigma(1;\vec{R}_i) + d\sigma(1;\vec{R}_j) - d\sigma_{\mathrm{SM}} + \sum_{k=1}^{m} (\alpha_{ki}^{-1} + \alpha_{kj}^{-1})^2(d\sigma'(2;\vec{R}_k) - d\sigma'(1;\vec{R}_k)) \\ &\quad + \sum_{k>l=1}^{m} (\alpha_{ki}^{-1} + \alpha_{kj}^{-1})(\alpha_{li}^{-1} + \alpha_{lj}^{-1})(d\sigma'(2;\vec{M}_{kl}) - d\sigma'(2;\vec{R}_k) - d\sigma'(2;\vec{R}_l) + d\sigma_{\mathrm{SM}}). \end{aligned}$$

[6]This applies for total cross sections, or bin by bin for differential cross sections.

The above results are found using

$$C_i C_j = \sum_{k=1}^{m} \alpha_{ik}\alpha_{jk} C'^2_k + \sum_{k>l=1}^{m} (\alpha_{ik}\alpha_{jl} + \alpha_{il}\alpha_{jk}) C'_k C'_l, \quad (24)$$

which simplifies for $i = j$ as

$$C_i^2 = \sum_{k=1}^{m} \alpha_{ik}^2 C'^2_k + 2 \sum_{k>l=1}^{m} \alpha_{ik}\alpha_{il} C'_k C'_l. \quad (25)$$

We illustrate the procedure and the utility of the results in this section by transforming from the Warsaw to the HISZ basis in Sec. IV.

III. FUTURE PROJECTIONS

In this section, we apply the results of the previous sections to projecting allowed regions for anomalous three-gauge-boson and Z-fermion couplings at a high-luminosity LHC (HL-LHC) and a potential 27 TeV collider (HE-LHC) under various assumptions about the systematic uncertainties. We have extended the POWHEG-BOX-V2 [36–38] implementation of the NLO QCD corrected predictions for the process $pp \to W^+W^- \to 4\ell$ [28,29],[7] which contains only the three-gauge-boson anomalous couplings, as originally found in Refs. [26,27] and implemented also in MCFM [39]. In our implementation in the POWHEG-BOX-V2, where we also include the anomalous Z-fermion couplings, there is the option to choose the order of the Λ^{-2n} expansion and the results can be generated using the effective interactions of Eqs. (2) and (3) or the Warsaw basis coefficients of Eq. (7). Our projections assume the Λ^{-4} expansion. Note that our extension works for the case of different-flavor leptonic final states. In the case of same-flavor charged leptons the contribution from ZZ production as well as the interference between W^+W^- and ZZ contributions should be included.

We apply the basic cuts,

$$p_T^\ell > 30 \text{ GeV}, \quad |\eta^\ell| < 2.5, \quad m_{\ell\ell} > 10 \text{ GeV}, \quad \not{E}_T > 20 \text{ GeV}, \quad \ell = e^\pm, \quad \mu^\mp, \quad (26)$$

where p_T^ℓ is charged lepton transverse momentum, η^ℓ is charged lepton rapidity, $m_{\ell\ell}$ is the invariant mass of the two charged leptons, and $\not{E}_T$ is the missing energy of the event. Since we do not include detector effects, in our case the missing transverse energy is the transverse energy of the two final state neutrinos. We work at the parton level and veto jets with

$$p_T^{\text{jet}} > 35 \text{ GeV}, \quad |\eta^{\text{jet}}| < 4.5, \quad (27)$$

where p_T^{jet} is the jet transverse momentum and η^{jet} is the jet rapidity. We further assume a 50% efficiency, in line with the experimental results of Ref. [40]. We use CT14QED inclusive PDFs [41], and take the renormalization/factorization scales equal to $\frac{M_{WW}}{2}$.

We assume a systematic uncertainty of $\delta_{\text{syst}} = 16\%$ and find the point where the systematic and statistical errors on the leading lepton p_T distribution are roughly equal, $\delta_{\text{stat}} \sim \delta_{\text{sys}}$. At this point, the uncertainties are systematics dominated and increased statistics provide diminishing returns. (In our figures, we investigate the impact of reducing the systematic error to $\delta_{\text{syst}} = 4\%$.) We define this point in terms of the integral over the leading lepton transverse momentum $p_T^{\ell,\text{lead}}$ above a cut $p_{T,\text{cut}}$,

$$\sigma(p_T^{\ell,\text{lead}} > p_{T,\text{cut}}) = \int_{p_{T,\text{cut}}} \frac{d\sigma}{dp_T^{\ell,\text{lead}}} dp_T^{\ell,\text{lead}}. \quad (28)$$

The p_T cut is defined to be the point where

$$\delta_{\text{sys}} = \delta_{\text{stat}} = \frac{1}{\sqrt{N}} = \frac{1}{\sqrt{L\sigma(p_T^{\ell,\text{lead}} > p_{T,\text{cut}})}}$$
$$\Rightarrow \sigma(p_T^{\ell,\text{lead}} > p_{T,\text{cut}}) = \frac{1}{L\delta_{\text{sys}}^2}. \quad (29)$$

L is the integrated luminosity and N is the number of events passing the cuts. This corresponds to roughly 38 events above the cut. Using integrated luminosities of 3 fb^{-1} at 14 TeV and 15 fb^{-1} at 27 TeV, we determine the p_T cuts:

$$14 \text{ TeV}: \; p_{T,\text{cut}} = 750 \text{ GeV}$$
$$27 \text{ TeV}: \; p_{T,\text{cut}} = 1350 \text{ GeV}. \quad (30)$$

Retaining $\delta_{\text{stat}} = 16\%$ with the corresponding p_T cuts of Eq. (30), we also consider the effect of reducing the systematic error to $\delta_{\text{sys}} = 4\%$.

We begin by setting the fermion couplings to their SM values. In this case the expansion to $\mathcal{O}(\Lambda^{-4})$ is the full amplitude squared, including both SM and SMEFT contributions. The projections at NLO QCD for 14 TeV are shown in Fig. 1 and for 27 TeV in Fig. 2, in black for $\delta_{\text{sys}} = 16\%$ and in red for $\delta_{\text{sys}} = 4\%$, named "3 GB." We see a significant improvement going from 14 to 27 TeV, while the improvement from reducing the systematic error, $\delta_{\text{sys}} = 16\% \to 4\%$, is marginal. Compared to Ref. [11], the improvement from 8 TeV to HL-LHC and HE-LHC is important. The coefficient λ^Z in particular is highly constrained, $|\lambda^Z| < 2 \times 10^{-3}$ at the HL-LHC and improved to $|\lambda^Z| < 6 \times 10^{-4}$ at the HE-LHC.

As demonstrated in Refs. [11–13,34,42], anomalous fermion couplings can have similar effects on the W^+W^- distributions as do the anomalous three-gauge-boson

[7] Our extension is built upon an updated private version. We thank Giulia Zanderighi for it.

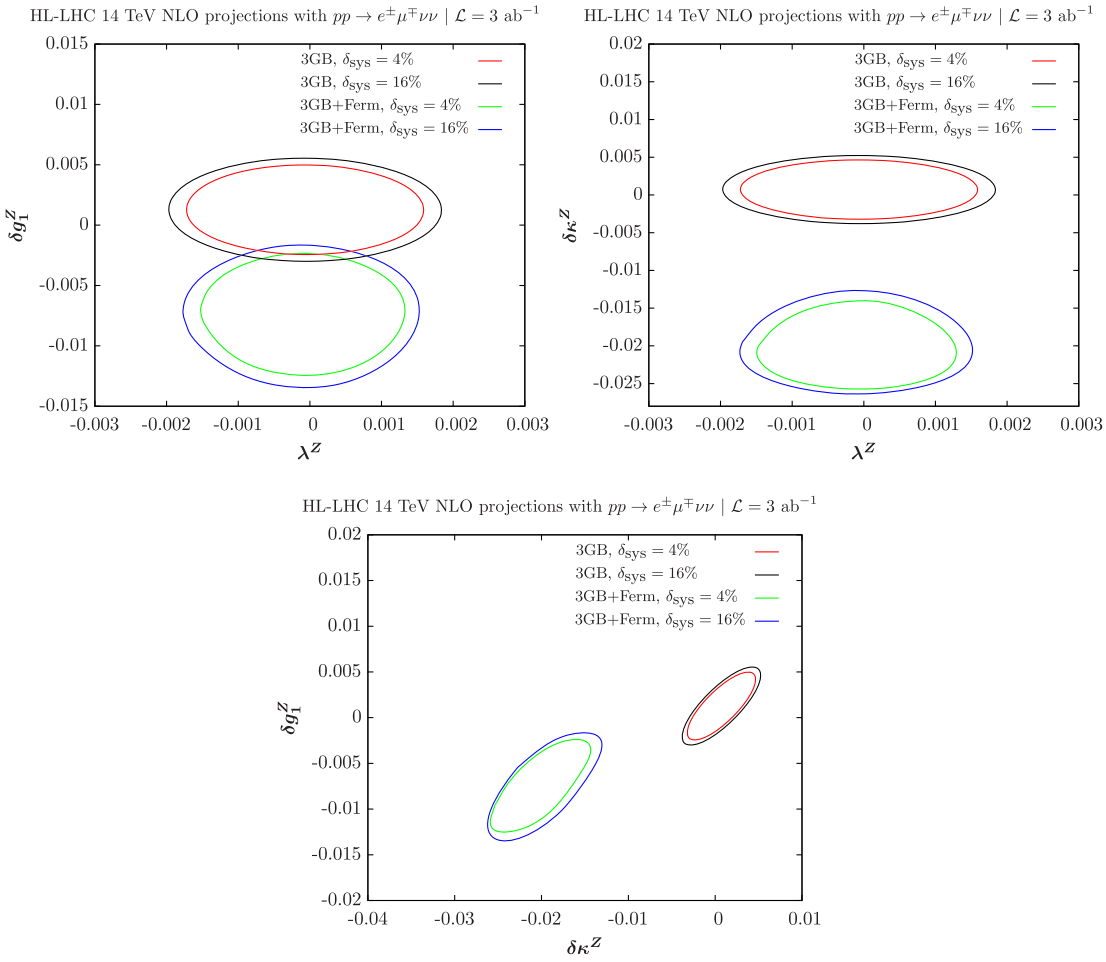

FIG. 1. Projections for the 14 TeV HE-LHC with 3 ab^{-1}. We take $p_{T,\rm cut} = 750$ GeV, corresponding to $\delta_{\rm stat} = 16\%$, and consider $\delta_{\rm sys} = 16\%$ and $\delta_{\rm sys} = 4\%$. The curves labeled 3 GB have SM Z-fermion couplings (black and red), while the curves labeled 3GB + Ferm allow the fermion couplings to vary within the 2σ region defined by Eq. (31) (blue and green). The standard cuts given in Eqs. (26) and (27) are applied.

couplings. At leading order, W^+W^- production proceeds through two s-channel diagrams with a photon or a Z and a t-channel diagram. The s-channel Z and t-channel diagrams are separately unitarity violating. In the SM, the violation is canceled once the diagrams are summed and the production rate is unitarized. However, the t-channel and s-channel diagrams have different dependencies on the Z-quark and W-quark couplings. Hence, if there are anomalous quark-gauge-boson couplings, the cancellation between the diagrams is spoiled and perturbative unitarity is violated. Although LEP strongly constrains these couplings [43–45], these constraints are at the Z-pole. At the higher energies of the LHC, the effects of the anomalous Z-quark and W-quark couplings grow with energy and their effect becomes important. While the perturbative unitarity violation is relevant for the W^+W^- production, for $W^\pm$ decays into leptons the leading order is one diagram and the process occurs at the W pole. Hence, there is no cancellation between diagrams to guarantee unitarity conservation and the process occurs at LEP energies. The very strong LEP constraints on W-lepton couplings [7] are relevant, so we set the lepton couplings to their SM values. However we consider the effects of anomalous Z-quark couplings, assuming flavor universality. We display in Figs. 1 and 2 the constraints that we obtain on the three-gauge-boson couplings while allowing for Z-quark anomalous couplings ranging over values that are constrained by global fits to LEP limits [43–45]:

$$\begin{aligned}
\delta g_L^{Zu} &= (-2.6 \pm 1.6) \times 10^{-3}, \\
\delta g_L^{Zd} &= (2.3 \pm 1) \times 10^{-3}, \\
\delta g_R^{Zu} &= (-3.6 \pm 3.5) \times 10^{-3}, \\
\delta g_R^{Zd} &= (16.0 \pm 5.2) \times 10^{-3}.
\end{aligned} \tag{31}$$

We allow the fermion couplings to vary within the 2σ limits given in Eq. (31). The curves are denoted "3GB + Ferm" in

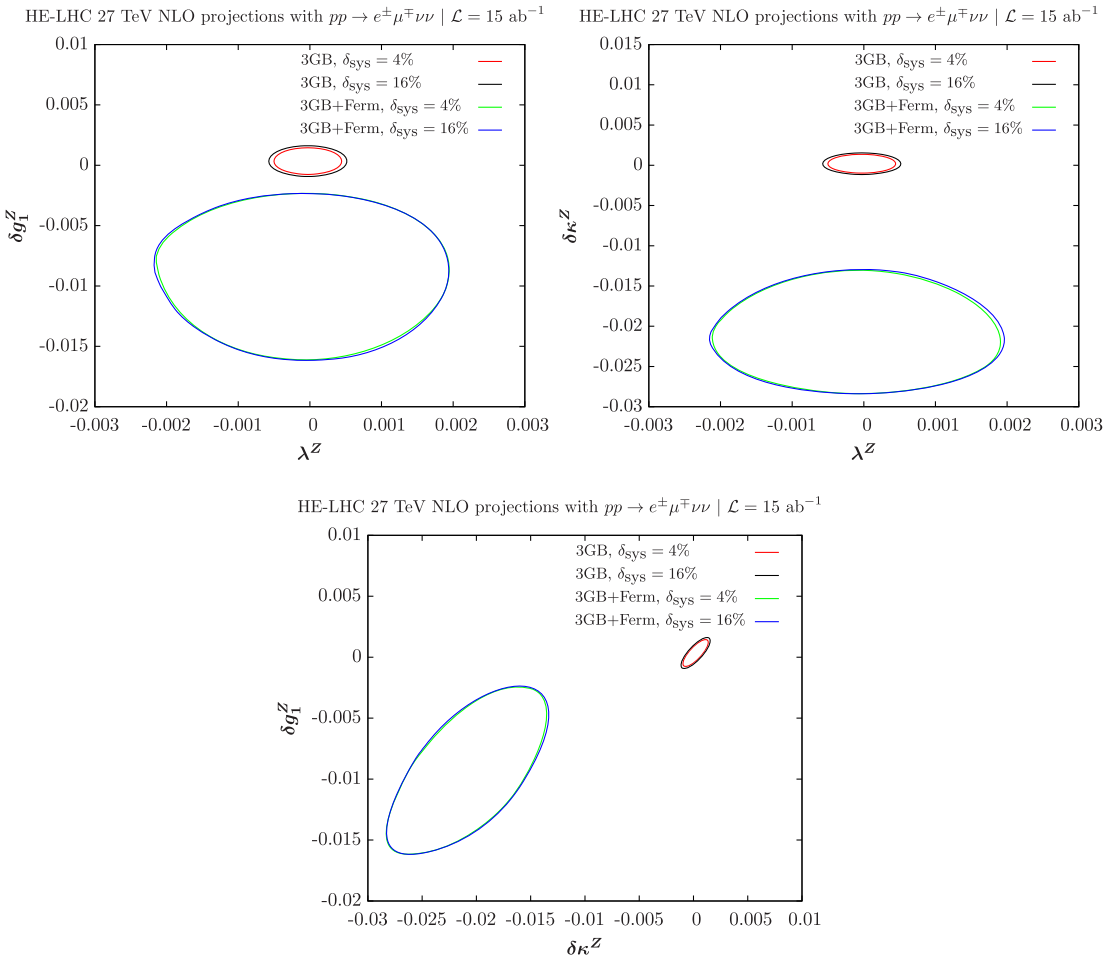

FIG. 2. Projections for the 27 TeV HE-LHC with 15 ab^{-1}. We take $p_{T,\rm cut} = 1350$ GeV, corresponding to $\delta_{\rm stat} = 16\%$, and consider $\delta_{\rm sys} = 16\%$ and $\delta_{\rm sys} = 4\%$. The curves labeled 3 GB have SM Z-fermion couplings (black and red), while the curves labeled 3GB + Ferm allow the fermion couplings to vary within the 2σ region defined by Eq. (31) (blue and green). The standard cuts given in Eqs. (26) and (27) are applied.

Figs. 1 and 2. They are displayed in green when assuming $\delta_{\rm sys} = 4\%$ and in blue when assuming $\delta_{\rm sys} = 16\%$. It is important to note that $\delta g_{L/R}^{Zd} = 0$ are not within the 2σ allowed range, and that the central values for all anomalous fermion couplings are nonzero. These observations are clearly translated into the allowed limits for the triple-gauge-boson anomalous couplings in Figs. 1 and 2 when scanning also over the anomalous fermion couplings in the range of Eq. (31). At 14 TeV the only (very limited) overlap between the 3 GB and 3GB + Ferm limits happens in the λ^Z-δg_1^Z plane. The nonzero central values of the anomalous fermion couplings interplay with the anomalous triple-gauge-boson couplings, which are nonzero for $\delta\kappa^Z$ and δg_1^Z as illustrated in particular in the third plot of Fig. 1. This is expected as the scan is performed relative to the SM value of the cross section: in order to get a cross section compatible with the SM while allowing at the same time nonzero anomalous fermion couplings, it is necessary to allow for nonzero anomalous triple-gauge-boson couplings. Comparing 14 to 27 TeV limits we also see that there is no noticeable improvement going from $\delta_{\rm sys} = 16\%$ down to $\delta_{\rm sys} = 4\%$. The 2σ bounds are already saturated and in particular indicate nonzero values for $\delta\kappa^Z$ and δg_Z^1 at more than 3σ when taking into account the anomalous fermion couplings according to the fit to LEP data as given in Eq. (31). The HE-LHC will thus be able to test the LEP fit and distinguish clearly between SM and non-SM Z-quark couplings, as the curves look quite different. An important implication of our study is that the anomalous fermion couplings have a major result on the allowed regions and cannot be neglected. When comparing our results with Ref. [13], a rough agreement is obtained. Our limits at the LHC are not exactly the same and the differences can be explained by the different assumptions in the two studies: the authors of Ref. [13] carried out a background + signal study at 13 TeV including also contributions from the $W^{\pm}Z$, while we work at 14 TeV without taking into account the backgrounds and focusing only on W^+W^-; the authors of Ref. [13] performed a fit on differential bins and profile over the variables not shown

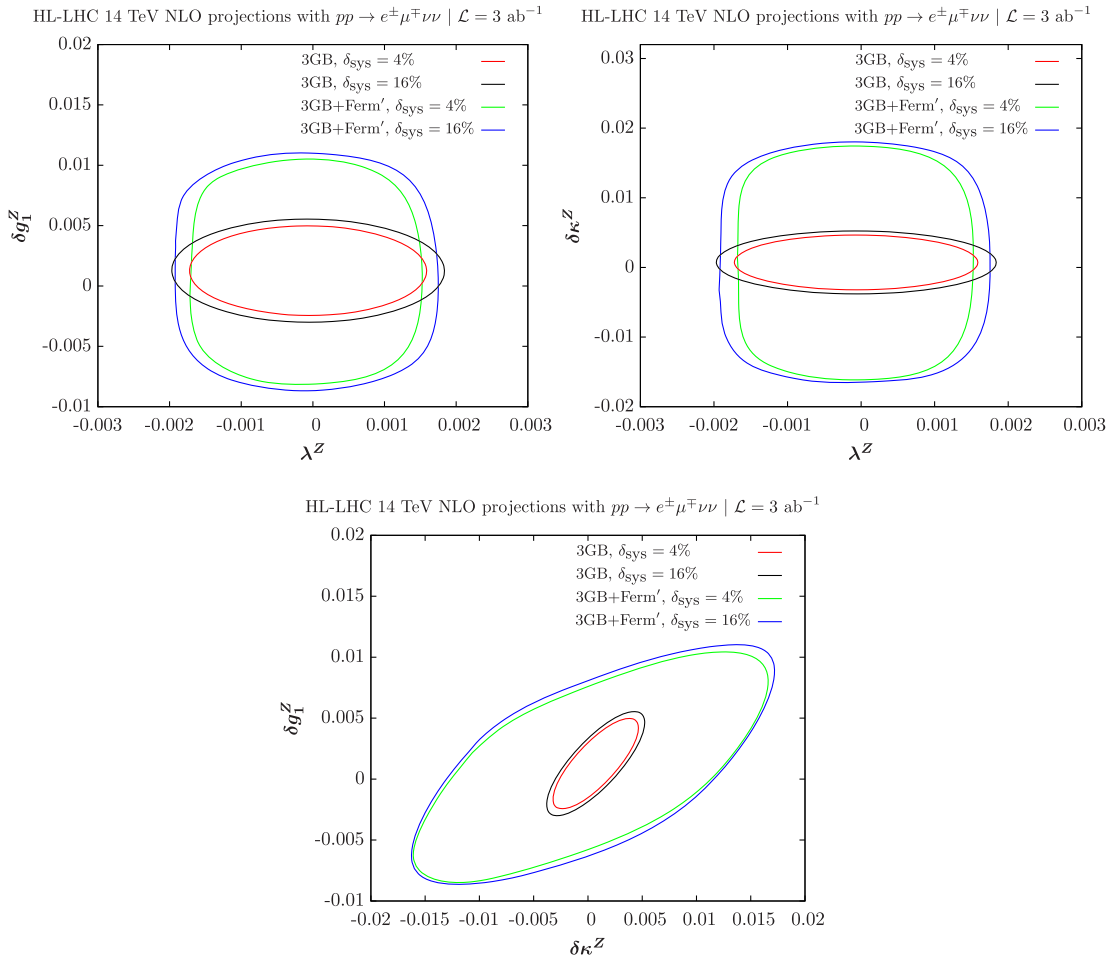

FIG. 3. Same as in Fig. 1, but with the fermion couplings constrained to vary around 0. The curves allowing for Z-quark coupling to vary around 0 within the 2σ limit in Eq. (32) are labeled 3GB + Ferm′. The standard cuts given in Eqs. (26) and (27) are applied.

in their plots, while we perform a fit on the last bin without profiling.

We have also performed a second scan where the Z-quark couplings are centered around their SM value, using the same 1σ limits as in Eq. (31),

$$\begin{aligned}\Delta(\delta g_L^{Zu}) &= 1.6 \times 10^{-3},\\ \Delta(\delta g_L^{Zd}) &= 1.0 \times 10^{-3},\\ \Delta(\delta g_R^{Zu}) &= 3.5 \times 10^{-3},\\ \Delta(\delta g_R^{Zd}) &= 5.2 \times 10^{-3}.\end{aligned} \tag{32}$$

The results are shown in Figs. 3 and 4 and the corresponding curves are labeled "3GB + Ferm′." The scans with only anomalous triple-gauge-boson couplings are given in black and red for $\delta_{\rm sys} = 16\%$ and 4% respectively; the scan with anomalous fermion couplings centered around 0 and with uncertainties defined according to Eq. (32) in addition are given in blue and green for $\delta_{\rm sys} = 16\%$ and 4% respectively. The curves 3GB + Ferm′ allow for a central value of zero, as expected. We still see that the shapes of the limits are no longer ellipses and that allowing for anomalous Z-quark couplings worsens the limits on the anomalous triple-gauge-boson couplings, especially at 27 TeV. We also see in Fig. 4 the same saturation as in Fig. 2 when comparing the two assumptions for the systematics; the improvement from 16% down to 4% is marginal. Negative values for $\delta\kappa^Z$ and δg_Z^1 are preferred over positive values. It is worth noticing that the 27 TeV limits for the 3GB + Ferm′ scenario are significantly better than those of the same scenario at 14 TeV when comparing Figs. 3 and 4, contrary to the case of 3GB + Ferm displayed in Figs. 1 and 2.

IV. 13 TEV DISTRIBUTIONS

In this section, we demonstrate the use of the primitive cross sections to compute K-factors and distributions in the presence of anomalous couplings. The primitive cross sections at 13 TeV [with and without the basic cuts of Eqs. (26) and (27)] are attached as Supplemental Material [46], including a variety of kinematic distributions of

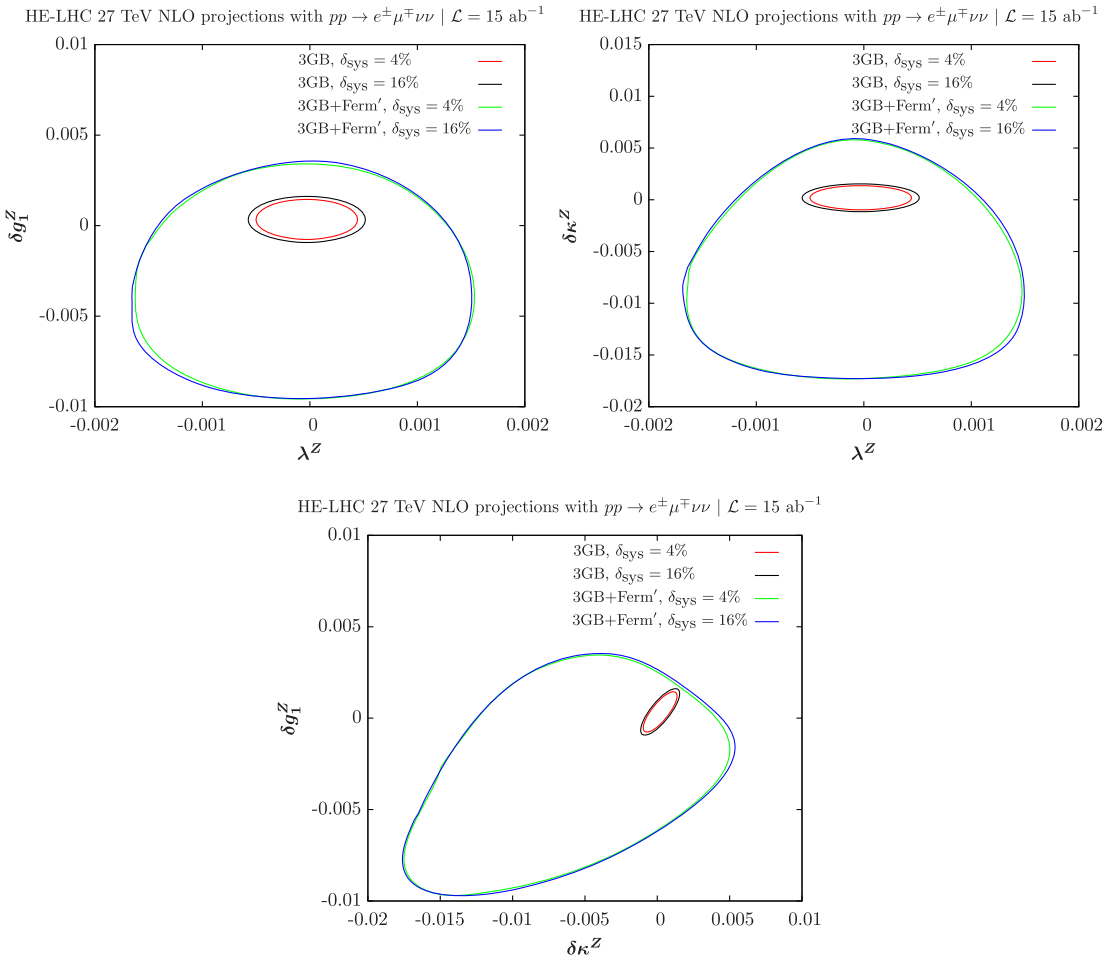

FIG. 4. Same as in Fig. 2, but with the fermion couplings constrained to vary around 0. The curves allowing for Z-quark coupling to vary around 0 within the 2σ limit in Eq. (32) are labeled 3GB + Ferm′. The standard cuts given in Eqs. (26) and (27) are applied.

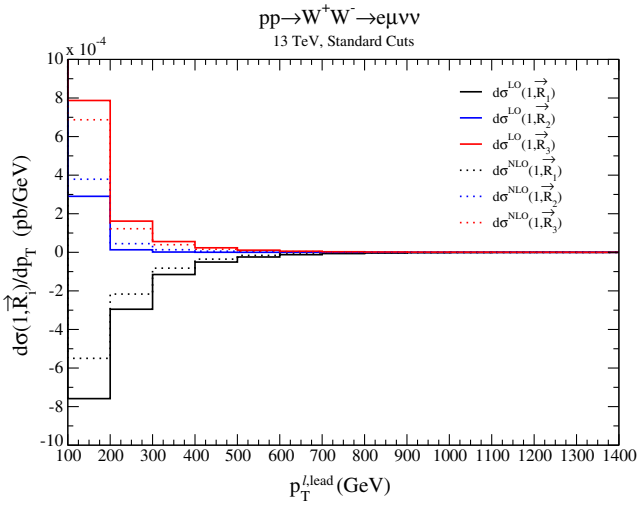

FIG. 5. Primitive cross sections relevant at $\mathcal{O}(\Lambda^{-2})$, with $\vec{C} = (\delta g_1^Z, \lambda^A, \delta\kappa^Z)$. $d\sigma(1,\vec{R}_i)$ is defined by Eq. (10). The standard cuts given in Eqs. (26) and (27) are applied.

interest. The goal is to enable rapid scans over anomalous couplings at NLO QCD. Our scheme is similar to the reweighting used in `MadGraph` [47]. We define a series of K-factors for the process $pp \to W^+W^- \to \mu^{\pm}e^{\mp}\nu\bar{\nu}$,

$$K_{\rm SM} = \frac{d\sigma^{\rm NLO}_{\rm SM}}{d\sigma^{\rm LO}_{\rm SM}}, \tag{33}$$

$$K^{(n)}_{\rm SMEFT} = \frac{d\sigma^{\rm NLO}_{\rm SMEFT}(C_1, C_2 \ldots C_m)}{d\sigma^{\rm LO}_{\rm SMEFT}(C_1, C_2, \ldots C_m)},$$
$$S^{(n)}_{\rm SMEFT} = \frac{d\sigma^{\rm NLO}_{\rm SMEFT}(C_1, C_2 \ldots C_m)}{d\sigma^{\rm NLO}_{\rm SM}}, \tag{34}$$

where $K^{(n)}_{\rm SMEFT}$ and $S^{(n)}_{\rm SMEFT}$ are evaluated in the SMEFT to $\mathcal{O}(\Lambda^{-2n})$ and LO and NLO refer to the order in QCD. The notation $d\sigma$ can represent either differential or total cross sections, where the numerators and denominators must be evaluated with identical cuts. Applying the cuts of Eqs. (26) and (27), the SM total cross sections are

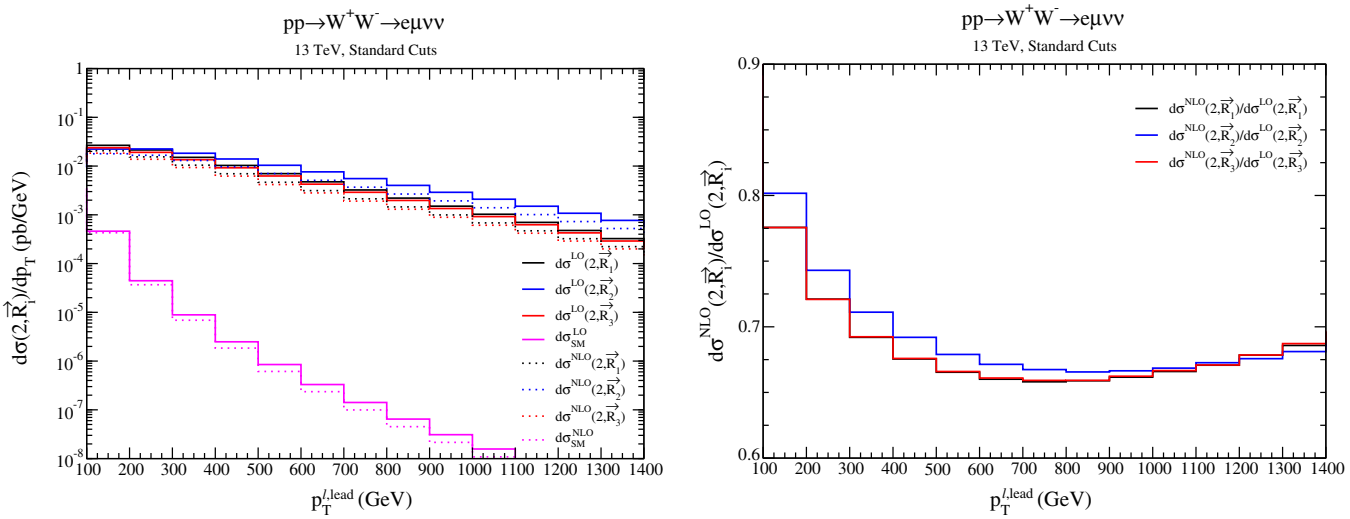

FIG. 6. Left: Primitive cross sections relevant at $\mathcal{O}(\Lambda^{-4})$, with $\vec{C} = (\delta g_1^Z, \lambda^A, \delta\kappa^Z)$. Right: Primitive cross sections relevant at $\mathcal{O}(\Lambda^{-4})$, normalized to the LO primitive cross sections. The black and red curves are almost indistinguishable. $d\sigma(2, \vec{R}_i)$ is defined in Eq. (10). The standard cuts given in Eqs. (26) and (27) are applied.

$$\sigma_{\rm SM}^{\rm LO} = 0.383 \text{ pb},$$
$$\sigma_{\rm SM}^{\rm NLO} = 0.400 \text{ pb}. \tag{35}$$

To $\mathcal{O}(\Lambda^{-2})$, the SMEFT K-factor is

$$K_{\rm SMEFT}^{(1)} = K_{\rm SM}[1 - \Sigma_i C_i (r_{1i}^{\rm LO} - r_{1i}^{\rm NLO})], \tag{36}$$

where we have normalized

$$r_{1i}^{\rm LO} = \frac{d\sigma^{\rm LO}(1;\vec{R}_i)}{d\sigma_{\rm SM}^{\rm LO}},$$
$$r_{1i}^{\rm NLO} = \frac{d\sigma^{\rm NLO}(1;\vec{R}_i)}{d\sigma_{\rm SM}^{\rm NLO}}, \tag{37}$$

where $d\sigma^{\rm LO}(1;\vec{R}_i)$ and $d\sigma^{\rm NLO}(1;\vec{R}_i)$ are the primitive functions defined in Eq. (10) evaluated at LO and NLO QCD, respectively. The primitive cross sections at $\mathcal{O}(\Lambda^{-2})$ that are relevant for the case where only the three-gauge-boson couplings are anomalous are shown in Fig. 5 for the leading lepton transverse momentum, $p_T^{\ell,\rm lead}$. To $\mathcal{O}(\Lambda^{-4})$, the analytic form for the $K_{\rm SMEFT}^{(2)}$ factor becomes rather complicated and we evaluate it numerically using Eq. (11). Figure 6 shows some of the primitive cross sections relevant at $\mathcal{O}(\Lambda^{-4})$. Note that the effects of the NLO corrections are not the same as those in the SM, although in both cases there is a strong dependence on $p_T^{\ell,\rm lead}$.

A useful form for expressing the results is

$$S_{\rm SMEFT}^{(2)} = (1 - \Sigma_{i=1}^m C_i) + \Sigma_i C_i \left[\frac{d\sigma^{\rm NLO}(1;\vec{R}_i)}{d\sigma_{\rm SM}^{\rm NLO}}\right],$$
$$S_{\rm SMEFT}^{(4)} = (1 - \Sigma_{i=1}^m C_i) + \Sigma_i C_i \left[\frac{d\sigma^{\rm NLO}(1;\vec{R}_i)}{d\sigma_{\rm SM}^{\rm NLO}}\right] + \Sigma_{i=1}^m C_i^2 \left[\frac{d\sigma^{\rm NLO}(2;\vec{R}_i) - d\sigma^{\rm NLO}(1;\vec{R}_i)}{d\sigma_{\rm SM}^{\rm NLO}}\right],$$
$$+ \Sigma_{i>j=1}^m C_i C_j \left[\frac{d\sigma^{\rm NLO}(2;\vec{M}_{ij}) - d\sigma^{\rm NLO}(2;\vec{R}_i) - d\sigma^{\rm NLO}(2;\vec{R}_j)}{d\sigma_{\rm SM}^{\rm NLO}} + 1\right], \tag{38}$$

where $d\sigma$ can be distributions or total cross sections. At 13 TeV with the usual cuts [see Eqs. (26) and (27)], the $S_{\rm SMEFT}^{(4)}$ factor for the total cross section is

$$S_{\rm SMEFT}^{(4)} = 1 + [-0.6305C_1 + 0.04881C_2 + 0.1767C_3 + 4.541C_4 - 0.3212C_5$$
$$- 4.723C_6 + 0.1327C_7] + 19.66C_1^2 + 21.93C_2^2 + 21.80C_3^2 + 32.97C_4^2$$
$$+ 36.92C_5^2 + 44.39C_6^2 + 25.45C_7^2 + \Sigma_{i>j=1}^m C_i C_j [X_{ij}], \tag{39}$$

where the values of X_{ij} are given in Table III and we define the coefficients, $\vec{C} = (\delta g_1^Z, \lambda^Z, \delta\kappa^Z, \delta g_L^{Zu}, \delta g_R^{Zu}, \delta g_L^{Zd}, \delta g_R^{Zd})$. The largest sensitivity of $S^{(4)}_{\rm SMEFT}$ is to the left-handed Z-quark couplings, as also observed in Ref. [13]. Equation (39) can be rescaled by the NLO SM total cross section, Eq. (35), to obtain numerical values to NLO for arbitrary SMEFT coefficients. Note that the numerical coefficients of Eq. (39) depend on the cuts.

For comparison, we present $S^{(4)}_{\rm SMEFT}$ in the HISZ basis of Eq. (8) using the primitive cross sections discussed above. Using the results of the previous section, $C_i = \Sigma_j \alpha_{ij} C'_j$, with

$$C_i = \begin{pmatrix} \delta g_1^Z \\ \delta\kappa_Z \\ \lambda_Z \end{pmatrix}, \qquad C'_i = \begin{pmatrix} \hat{f_W} = f_W(\frac{M_Z^2}{\Lambda^2}) \\ \hat{f_B} = f_B(\frac{M_Z^2}{\Lambda^2}) \\ \hat{f}_{WWW} = f_{WWW}\left(\frac{M_Z^2}{\Lambda^2}\right) \end{pmatrix}, \qquad \alpha = \begin{pmatrix} \frac{1}{2} & 0 & 0 \\ \frac{c_W^2}{2} & -\frac{s_W^2}{2} & 0 \\ 0 & 0 & \frac{3g^2c_W^2}{4} \end{pmatrix}, \tag{40}$$

and $C_i = C'_i$, $i = 4$–7. The $S^{(4)}_{\rm SMEFT}$ factor in a transformed basis is

$$\begin{aligned} S^{(4)}_{\rm SMEFT} &= (1 - \Sigma_{i,k=1}^m C'_i\alpha_{ki}) + \Sigma_{i,k=1}^m C'_i\alpha_{ki}\left[\frac{d\sigma^{\rm NLO}(1;\vec{R}_k)}{d\sigma^{\rm NLO}_{\rm SM}}\right] \\ &+ \Sigma_{i=1}^m C_i'^2\left\{\Sigma_{k=1}^m \alpha_{ki}^2\left[\frac{d\sigma^{\rm NLO}(2;\vec{R}_k) - d\sigma^{\rm NLO}(1;\vec{R}_k)}{d\sigma^{\rm NLO}_{\rm SM}}\right]\right. \\ &\left. + \Sigma_{l=1}^m\Sigma_{k=l+1}^m \alpha_{ki}\alpha_{li}\left[\frac{d\sigma^{\rm NLO}(2,\vec{M}_{kl}) - d\sigma^{\rm NLO}(2;\vec{R}_k) - d\sigma^{\rm NLO}(2;\vec{R}_l)}{d\sigma^{\rm NLO}_{\rm SM}} + 1\right]\right\} \\ &+ \Sigma_{j=1}^m\Sigma_{i=j+1}^m C'_iC'_j\left\{\Sigma_{k=1}^m 2\alpha_{ki}\alpha_{kj}\left[\frac{d\sigma^{\rm NLO}(2;\vec{R}_k) - d\sigma^{\rm NLO}(1;\vec{R}_k)}{d\sigma^{\rm NLO}_{\rm SM}}\right]\right. \\ &+ \Sigma_{l=1}^m\Sigma_{k=l+1}^m(\alpha_{kj}\alpha_{li} + \alpha_{ki}\alpha_{lj}) \\ &\left.\cdot\left[\frac{d\sigma^{\rm NLO}(2;\vec{M}_{kl}) - d\sigma^{\rm NLO}(2;\vec{R}_k) - d\sigma^{\rm NLO}(2;\vec{R}_l)}{d\sigma^{\rm NLO}_{\rm SM}} + 1\right]\right\}. \end{aligned} \tag{41}$$

For $i, j = 4$–7, $\alpha_{ij} = \delta_{ij}$. The primitive cross sections $d\sigma^{\rm NLO}(n,\vec{R}_i)$ and $d\sigma^{\rm NLO}(n,\vec{M}_{ij})$ are defined in Eqs. (10) and (12) and are evaluated in the original anomalous coupling basis.

For the total cross section in the HISZ basis applying our basic cuts in Eqs. (26) and (27) with $\vec{C}' = (\hat{f}_W, \hat{f}_B, \hat{f}_{WWW}, \delta g_L^{Zu}, \delta g_R^{Zu}, \delta g_L^{Zd}, \delta g_R^{Zd})$ and $\Lambda = 1$ TeV,

$$\begin{aligned} S^{(4)}_{\rm SMEFT,HISZ} &= 1 + [-0.4059C'_1 - 1.115C'_2 - 0.7189C'_3 \\ &+ 4.541C'_4 - 0.3211C'_5 - 4.723C'_6 + 0.1327C'_7] \\ &+ 8.687C_1'^2 + .2639C_2'^2 + 1.2C_3'^2 + 32.97C_4'^2 \\ &+ 36.92C_5'^2 + 44.39C_6'^2 + 25.45C_7'^2 + \Sigma_{i>j=1}^m C'_iC'_j[\hat{X}_{ij}], \end{aligned} \tag{42}$$

TABLE III. Coefficients defined in Eq. (39) with $\vec{C} = (\delta g_1^Z, \lambda^Z, \delta\kappa^Z, \delta g_L^{Zu}, \delta g_R^{Zu}, \delta g_L^{Zd}, \delta g_R^{Zd})$. The standard cuts given in Eqs. (26) and (27) are applied.

X_{ij}	2	3	4	5	6	7
1	2.211	−31.35	−14.67	32.20	36.82	−10.77
2		−4.963	−2.372	−0.1275	2.931	0.055 77
3			−13.49	−48.49	−14.66	9.676
4				−0.026 63	−15.00	−0.026 611
5					−0.001 471	−0.003 671
6						0.000 303 3

TABLE IV. HISZ basis coefficients defined in Eq. (42) with $\vec{C}' = (\hat{f}_W, \hat{f}_B, \hat{f}_{WWW}, \delta g_L^{Zu}, \delta g_R^{Zu}, \delta g_L^{Zd}, \delta g_R^{Zd})$ and $\Lambda = 1$ TeV. The standard cuts given in Eqs. (26) and (27) are applied.

$\hat{X}_{ij}$	2	3	4	5	6	7
1	−1.447	−3.917	−14.67	32.20	36.82	−10.77
2		1.178	−2.372	−0.1275	2.931	0.055 77
3			−13.49	−48.49	−14.66	9.676
4				−0.026 63	−15.00	−0.02611
5					−0.001 471	−0.003 671
6						0.000 303 3

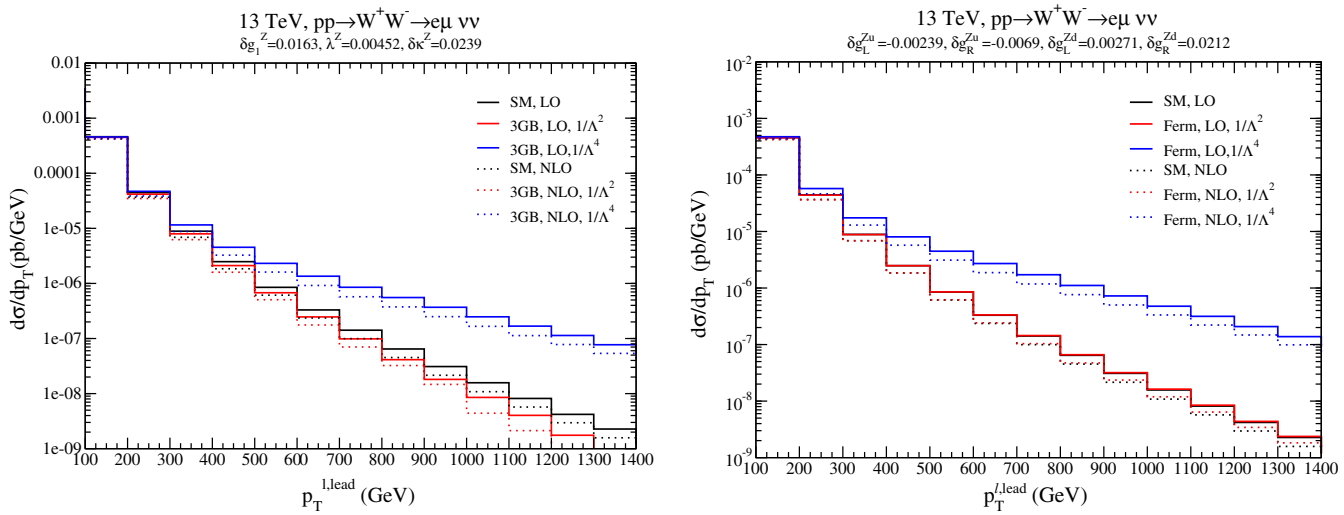

FIG. 7. Distribution of the leading charged lepton p_T in a scenario with only anomalous three-gauge-boson couplings (left) and only anomalous Z-fermion couplings (right) to $\mathcal{O}(\Lambda^{-2})$ and $\mathcal{O}(\Lambda^{-4})$ at LO and NLO QCD. The SM, LO and Ferm, LO, and $1/\Lambda^2$ curves on the right are indistinguishable. The standard cuts given in Eqs. (26) and (27) are applied.

where the values of $\hat{X}_{ij}$ are given in Table IV.

The primitive cross sections can also be used to study distributions with arbitrary SMEFT coefficients and we show some sample results for the transverse momentum of the leading charged lepton, $p_T^{\ell,\mathrm{lead}}$, and for the invariant mass distribution of the charged leptons, $m_{\ell\ell}$. In Fig. 7, we show the distribution of the leading lepton p_T in a scenario with only anomalous three-gauge-boson couplings (left) and with only anomalous Z-quark couplings (right). The values of the coefficients were chosen to be allowed by experimental limits from W^+W^- pair production [40,48] and from fits to LEP data [7], and to give similar p_T distributions. It is apparent that the anomalous three-gauge-boson-only and anomalous-Z-fermion-only scenarios cannot be distinguished by studying the p_T distributions alone and that the dominant effects come from the Λ^{-4} contributions. The NLO effects decrease the rate at high p_T for the anomalous three-gauge-boson couplings and increase it for anomalous Z-fermion couplings.

Figures 8 and 9 show the variables of Eq. (34). The $S^{(n)}_{\mathrm{SMEFT}}$ variable compares the SMEFT distributions with those of the SM, demonstrating the dominance of the Λ^{-4} terms at large p_T. SM and SMEFT K-factors are shown in Fig. 9 and it is clear that the SM and SMEFT scale

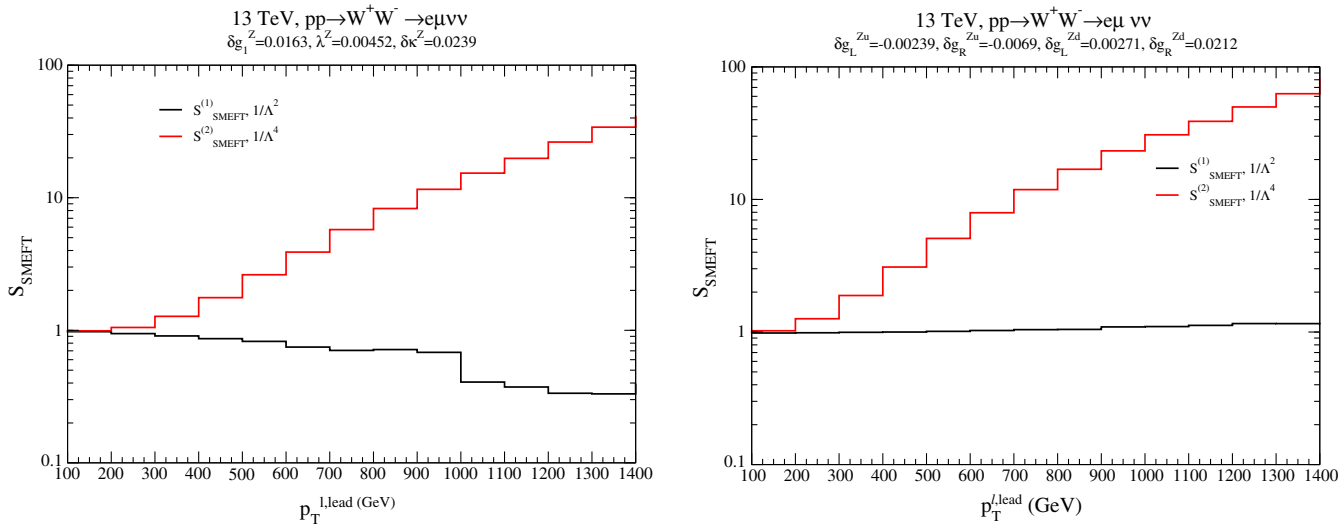

FIG. 8. Comparison of the S factors of Eq. (34) for the SM and SMEFT in the anomalous three-gauge-boson-only scenario (left) and anomalous-fermion-only scenario (right) at $\mathcal{O}(\Lambda^{-2})$ and $\mathcal{O}(\Lambda^{-4})$. The standard cuts given in Eqs. (26) and (27) are applied.

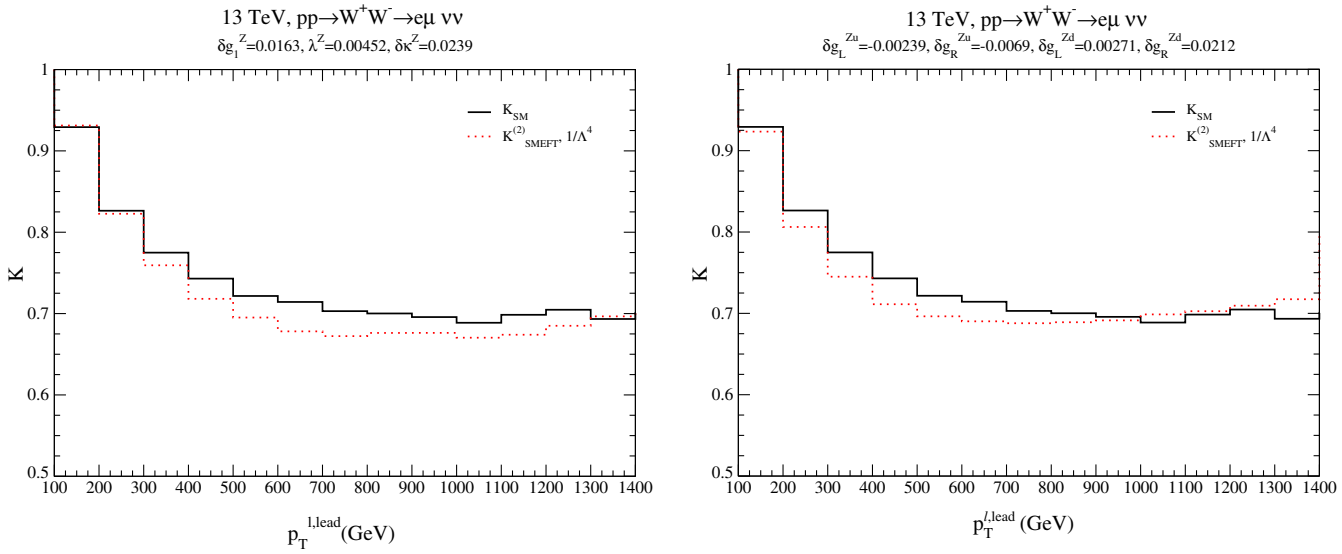

FIG. 9. Comparison of the K-factors of Eq. (34) for the SM and SMEFT in the anomalous three-gauge-boson-only scenario (left) and anomalous-fermion-only scenario (right). The standard cuts given in Eqs. (26) and (27) are applied.

similarly with small variations. Similarly, the K-factors for the anomalous-fermion-only scenario (Fig. 9, right) and the anomalous-3 GB-only scenario (Fig. 9, left) are also similar with small variations. We note that this is for specific choices of the anomalous couplings and for different choices the K-factors have to be checked using the primitive cross sections.

In Fig. 10, we show the invariant mass distribution of the charged leptons in a scenario with only anomalous three-gauge-boson couplings (left) and with only anomalous Z-quark couplings (right). As is the case with the p_T distributions, the dominant effect arises from the Λ^{-4} contributions. Figures 11 and 12 show the variables of Eq. (34). The $S^{(n)}_{\mathrm{SMEFT}}$ variable compares the SMEFT distributions with those of the SM, again showing the large effects from the $\mathcal{O}(\Lambda^{-4})$ terms. SM and SMEFT K-factors are shown in Fig. 12 and are quite similar to each other.

In Ref. [25], the authors computed the NLO QCD (along with the NLO electroweak) corrections to gauge boson pair production when the fermion couplings take their SM values. Our results are qualitatively similar to theirs for the scenario with only anomalous three-gauge-boson couplings.

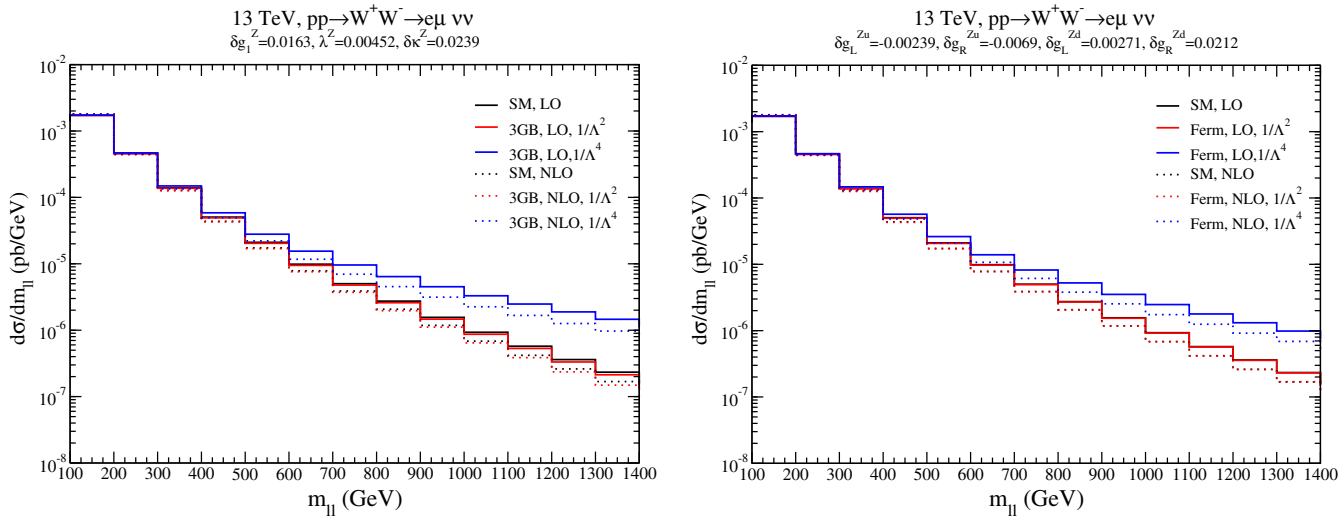

FIG. 10. Invariant mass distribution in a scenario with only anomalous three-gauge-boson couplings (left) and only anomalous fermion couplings (right) to $\mathcal{O}(\Lambda^{-2})$ and $\mathcal{O}(\Lambda^{-4})$ at LO and NLO QCD. The standard cuts given in Eqs. (26) and (27) are applied.

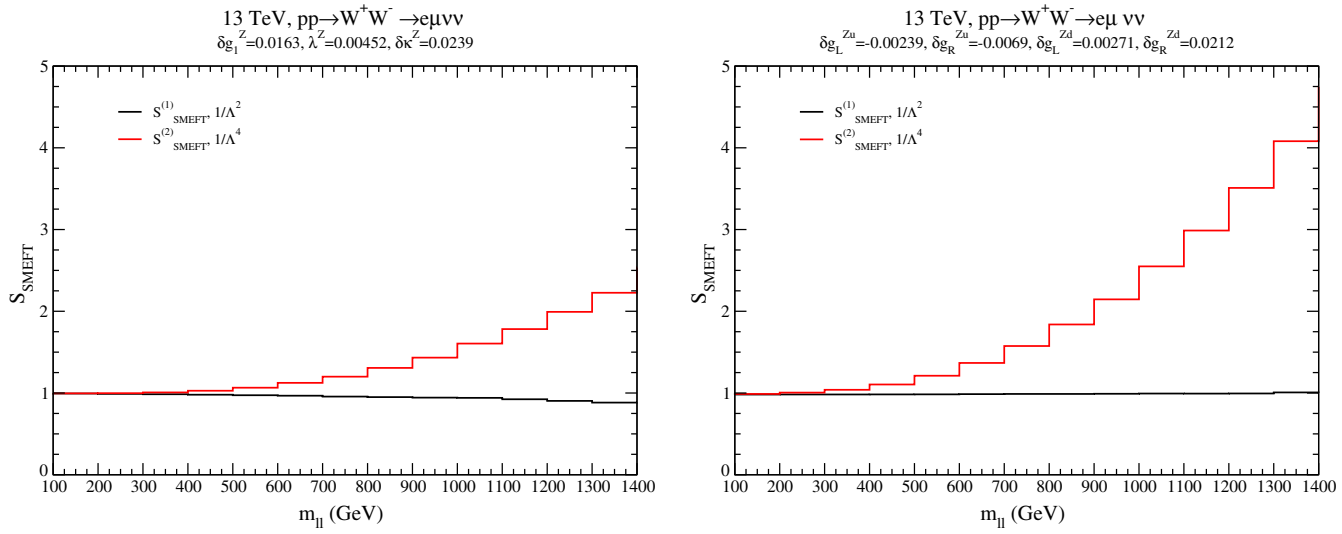

FIG. 11. Comparison of the S factors of Eq. (34) for the SM and SMEFT in the anomalous three-gauge-boson-only scenario (left) and anomalous-fermion-only scenario (right). The standard cuts given in Eqs. (26) and (27) are applied.

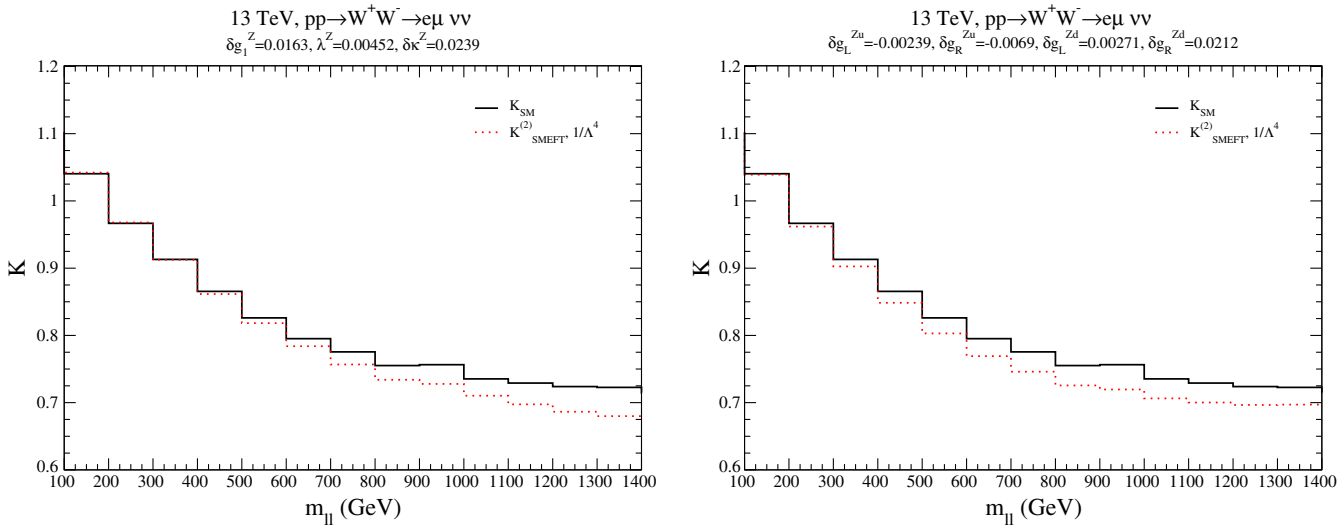

FIG. 12. Comparison of the K-factors of Eq. (34) for the SM and SMEFT in the anomalous three-gauge-boson-only scenario (left) and anomalous-fermion-only scenario (right). The standard cuts given in Eqs. (26) and (27) are applied.

V. CONCLUSIONS

We have extended our previous NLO calculation of the contribution of anomalous couplings to $pp \to W^+W^-$ to include the leptonic decays, $pp \to W^+W^- \to \mu^\pm e^\mp \nu\bar{\nu}$ and implemented the results in the POWHEG-BOX. The primitive cross sections at 13 TeV for a variety of observables are posted at [49]. The most important implication of our results is the interplay between anomalous Z-quark couplings and anomalous three-gauge-boson couplings requiring global fits to both fermion and gauge couplings in order to obtain reliable results. Our NLO results at 13 TeV are presented in terms of primitive cross sections allowing for rapid scans over anomalous couplings in an arbitrary basis.

ACKNOWLEDGMENTS

We thank Giulia Zanderighi and Paolo Nason for discussions about the private updated version of their code. We also thank Barbara Jäger for valuable discussions. S. D. is supported by the United States Department of Energy under Grant No. DE-SC0012704 and is grateful to the University of Tübingen, where this work was started. I. M. L. is supported in part by United States Department of Energy Grant No. DE-SC0017988. J. B. acknowledges the

support from the Carl-Zeiss foundation. Parts of this work were performed thanks to the support of the State of Baden-Württemberg through bwHPC and the DFG through Grant No. INST 39/963-1 FUGG. The data to reproduce the plots have been uploaded with the arXiv submission and are available upon request.

[1] S. Dawson, C. Englert, and T. Plehn, Higgs physics: It ain't over till it's over, arXiv:1808.01324.
[2] G. Aad *et al.* (ATLAS and CMS Collaborations), Measurements of the Higgs boson production and decay rates and constraints on its couplings from a combined ATLAS and CMS analysis of the LHC pp collision data at $\sqrt{s} = 7$ and 8 TeV, J. High Energy Phys. 08 (2016) 045.
[3] A. Butter, O. J. P. Eboli, J. Gonzalez-Fraile, M. C. Gonzalez-Garcia, T. Plehn, and M. Rauch, The gauge-Higgs legacy of the LHC Run I, J. High Energy Phys. 07 (2016) 152.
[4] M. Aaboud *et al.* (ATLAS Collaboration), Measurement of the Higgs boson coupling properties in the $H \to ZZ^* \to 4\ell$ decay channel at $\sqrt{s} = 13$ TeV with the ATLAS detector, J. High Energy Phys. 03 (2018) 095.
[5] M. Aaboud *et al.* (ATLAS Collaboration), Measurements of Higgs boson properties in the diphoton decay channel with 36 fb^{-1} of pp collision data at $\sqrt{s} = 13$ TeV with the ATLAS detector, Phys. Rev. D **98**, 052005 (2018).
[6] A. M. Sirunyan *et al.* (CMS Collaboration), Combined measurements of Higgs boson couplings in proton-proton collisions at $\sqrt{s} = 13$ TeV, arXiv:1809.10733.
[7] S. Schael *et al.* (DELPHI, OPAL, LEP Electroweak, ALEPH, and L3 Collaborations), Electroweak measurements in electron-positron collisions at W-boson-pair energies at LEP, Phys. Rep. **532**, 119 (2013).
[8] M. J. Duncan, G. L. Kane, and W. W. Repko, WW physics at future colliders, Nucl. Phys. **B272**, 517 (1986).
[9] K. Hagiwara, R. D. Peccei, D. Zeppenfeld, and K. Hikasa, Probing the weak boson sector in $e^+e^- \to W^+W^-$, Nucl. Phys. **B282**, 253 (1987).
[10] Z. Zhang, Time to Go Beyond Triple-Gauge-Boson-Coupling Interpretation of W Pair Production, Phys. Rev. Lett. **118**, 011803 (2017).
[11] J. Baglio, S. Dawson, and I. M. Lewis, An NLO QCD effective field theory analysis of W^+W^- production at the LHC including fermionic operators, Phys. Rev. D **96**, 073003 (2017).
[12] A. Alves, N. Rosa-Agostinho, O. J. P. Eboli, and M. C. Gonzalez-Garcia, Effect of fermionic operators on the gauge legacy of the LHC Run I, Phys. Rev. D **98**, 013006 (2018).
[13] C. Grojean, M. Montull, and M. Riembau, Diboson at the LHC vs LEP, arXiv:1810.05149.
[14] W. Buchmuller and D. Wyler, Effective Lagrangian analysis of new interactions and flavor conservation, Nucl. Phys. **B268**, 621 (1986).
[15] B. Grzadkowski, M. Iskrzynski, M. Misiak, and J. Rosiek, Dimension-six terms in the Standard Model Lagrangian, J. High Energy Phys. 10 (2010) 085.
[16] J. Bellm, S. Gieseke, N. Greiner, G. Heinrich, S. Platzer, C. Reuschle, and J. F. von Soden-Fraunhofen, Anomalous coupling, top-mass and parton-shower effects in W^+W^- production, J. High Energy Phys. 05 (2016) 106.
[17] T. Gehrmann, M. Grazzini, S. Kallweit, P. Maierhofer, A. von Manteuffel, S. Pozzorini, D. Rathlev, and L. Tancredi, W^+W^- Production at Hadron Colliders in Next to Next to Leading Order QCD, Phys. Rev. Lett. **113**, 212001 (2014).
[18] M. Grazzini, S. Kallweit, S. Pozzorini, D. Rathlev, and M. Wiesemann, W^+W^- production at the LHC: Fiducial cross sections and distributions in NNLO QCD, J. High Energy Phys. 08 (2016) 140.
[19] S. Dawson, P. Jaiswal, Y. Li, H. Ramani, and M. Zeng, Resummation of jet veto logarithms at N^{3}LL$_a$ + NNLO for W^+W^- production at the LHC, Phys. Rev. D **94**, 114014 (2016).
[20] K. Hamilton, T. Melia, P. F. Monni, E. Re, and G. Zanderighi, Merging WW and WW + jet with MINLO, J. High Energy Phys. 09 (2016) 057.
[21] A. Bierweiler, T. Kasprzik, and J. H. Kuhn, Vector-boson pair production at the LHC to $\mathcal{O}(\alpha^3)$ accuracy, J. High Energy Phys. 12 (2013) 071.
[22] J. Baglio, L. D. Ninh, and M. M. Weber, Massive gauge boson pair production at the LHC: A next-to-leading order story, Phys. Rev. D **88**, 113005 (2013); Erratum, Phys. Rev. D **94**, 099902(E) (2016).
[23] B. Biedermann, M. Billoni, A. Denner, S. Dittmaier, L. Hofer, B. Jaeger, and L. Salfelder, Next-to-leading-order electroweak corrections to $pp \to W^+W^- \to 4$ leptons at the LHC, J. High Energy Phys. 06 (2016) 065.
[24] J. M. Campbell, R. K. Ellis, and C. Williams, Vector boson pair production at the LHC, J. High Energy Phys. 07 (2011) 018.
[25] M. Chiesa, A. Denner, and J.-N. Lang, Anomalous triple-gauge-boson interactions in vector-boson pair production with RECOLA2, Eur. Phys. J. C **78**, 467 (2018).
[26] L. J. Dixon, Z. Kunszt, and A. Signer, Helicity amplitudes for O(α_s) production of W^+W^-, $W^\pm Z$, ZZ, $W^\pm\gamma$, or $Z\gamma$ pairs at hadron colliders, Nucl. Phys. **B531**, 3 (1998).
[27] L. J. Dixon, Z. Kunszt, and A. Signer, Vector boson pair production in hadronic collisions at order α_s: Lepton correlations and anomalous couplings, Phys. Rev. D **60**, 114037 (1999).
[28] T. Melia, P. Nason, R. Rontsch, and G. Zanderighi, W^+W^-, WZ and ZZ production in the POWHEG BOX, J. High Energy Phys. 11 (2011) 078.
[29] P. Nason and G. Zanderighi, W^+W^-, WZ and ZZ production in the POWHEG-BOX-V2, Eur. Phys. J. C **74**, 2702 (2014).
[30] http://powhegbox.mib.infn.it.
[31] A. Biekötter, D. Gonçalves, T. Plehn, M. Takeuchi, and D. Zerwas, The global Higgs picture at 27 TeV, arXiv:1811.08401.

[32] K. J. F. Gaemers and G. J. Gounaris, Polarization amplitudes for $e^+e^- \to W^+W^-$ and $e^+e^- \to ZZ$, Z. Phys. C **1**, 259 (1979).
[33] A. Azatov, R. Contino, C. S. Machado, and F. Riva, Helicity selection rules and noninterference for BSM amplitudes, Phys. Rev. D **95**, 065014 (2017).
[34] A. Falkowski, M. Gonzalez-Alonso, A. Greljo, D. Marzocca, and M. Son, Anomalous triple gauge couplings in the effective field theory approach at the LHC, J. High Energy Phys. 02 (2017) 115.
[35] A. Dedes, W. Materkowska, M. Paraskevas, J. Rosiek, and K. Suxho, Feynman rules for the standard model effective field theory in R_ξ-gauges, J. High Energy Phys. 06 (2017) 143.
[36] P. Nason, A new method for combining NLO QCD with shower Monte Carlo algorithms, J. High Energy Phys. 11 (2004) 040.
[37] S. Frixione, P. Nason, and C. Oleari, Matching NLO QCD computations with parton shower simulations: The POWHEG method, J. High Energy Phys. 11 (2007) 070.
[38] S. Alioli, P. Nason, C. Oleari, and E. Re, A general framework for implementing NLO calculations in shower Monte Carlo programs: The POWHEG BOX, J. High Energy Phys. 06 (2010) 043.
[39] J. M. Campbell and R. K. Ellis, An update on vector boson pair production at hadron colliders, Phys. Rev. D **60**, 113006 (1999).
[40] G. Aad *et al.* (ATLAS Collaboration), Measurement of total and differential W^+W^- production cross sections in proton-proton collisions at $\sqrt{s} = 8$ TeV with the ATLAS detector and limits on anomalous triple-gauge-boson couplings, J. High Energy Phys. 09 (2016) 029.
[41] C. Schmidt, J. Pumplin, D. Stump, and C. P. Yuan, CT14QED parton distribution functions from isolated photon production in deep inelastic scattering, Phys. Rev. D **93**, 114015 (2016).
[42] D. Liu and L.-T. Wang, Precision measurement with diboson at the LHC, arXiv:1804.08688.
[43] A. Falkowski and F. Riva, Model-independent precision constraints on dimension-6 operators, J. High Energy Phys. 02 (2015) 039.
[44] A. Falkowski, M. Gonzalez-Alonso, and K. Mimouni, Compilation of low-energy constraints on 4-fermion operators in the SMEFT, J. High Energy Phys. 08 (2017) 123.
[45] L. Berthier, M. Bjorn, and M. Trott, Incorporating doubly resonant $W^\pm$ data in a global fit of SMEFT parameters to lift flat directions, J. High Energy Phys. 09 (2016) 157.
[46] See Supplemental Material at http://link.aps.org/supplemental/10.1103/PhysRevD.99.035029 which contains primitive amplitudes for W^+W^- production at 13 TeV at the LHC.
[47] O. Mattelaer, On the maximal use of Monte Carlo samples: Re-weighting events at NLO accuracy, Eur. Phys. J. C **76**, 674 (2016).
[48] V. Khachatryan *et al.* (CMS Collaboration), Measurement of the W^+W^- cross section in pp collisions at $\sqrt{s} = 8$ TeV and limits on anomalous gauge couplings, Eur. Phys. J. C **76**, 401 (2016).
[49] https://quark.phy.bnl.gov/Digital_Data_Archive/dawson/ww_18.